Available online at www.sciencedirect.com
SCIENCE DIRECT®
Journal of Nuclear Materials 335 (2004) 520–528
journal of nuclear materials
www.elsevier.com/locate/jnucmat

Micro-texture of extruded Zr–2.5Nb tubes

R.A. Holt *, Pingshun Zhao

Department of Mechanical and Materials Engineering, Queen's University, McLaughlin Hall, 130 Stuart Street, Kingston Ontario, Canada K7L 3N6

Received 21 January 2004; accepted 14 July 2004

Abstract

We report the micro-texture of two extruded Zr–2.5Nb tubes determined using scanning electron microscopy combined with electron back-scattering diffraction (SEM/EBSD) and transmission electron microscopy and selected area diffraction (TEM/SAD). The pole figures determined by SEM/EBSD correspond well with bulk pole figures previously determined by X-ray diffraction (XRD). Three components of texture are seen to correlate with the shape and morphology of the α-grains and their contained dislocation substructures. The first component corresponds to elongated alpha grains containing a high density of **a** and **c** + **a** dislocations in which the **c**-axis is oriented at a relatively high angle to the long dimension of the α-grains as viewed in transverse section; these grains comprise a texture component with the **c**-axes in the radial transverse plane, tilted towards the radial direction. The second component corresponds to elongated α-grains containing a low dislocation density in which the **c**-axis is oriented parallel to the long dimension of the alpha grains: these grains also comprise a texture component with the **c**-axis in the radial/transverse plane, but predominantly in the transverse direction. The final component corresponds to colonies of Widmanstätten-like α-grains that are transformed from the β-phase: the majority of these grains have their **c**-axes in the axial direction. These grain have very low dislocation densities and are probably developed during cooling, after extrusion.

1. Introduction

Zr–2.5Nb is used in the extruded and cold-worked condition for pressure tubes in CANDU© reactors. Many of the properties of the material are associated with the crystallographic texture produced during the extrusion stage (extrusion ratio of 10:1, preheat temperature of 1090 K). In standard pressure tubes, this comprises a predominantly transverse distribution of the basal plane normals, sometimes with a weak component down the tube axis [1,2]. The typical manufacturing route for cold-worked and stress-relieved fuel cladding (repetitive cold-working and intermediate annealing after extrusion, with a high ratio of wall reduction to diameter reduction on the final pass) gives a distribution in which the basal plane normals are closer to the radial direction [3,4]. Some of the properties of this alloy that are technologically important, such as delayed hydride cracking and irradiation induced deformation, have been demonstrated experimentally and theoretically to be controlled by the texture [5–8].

The Zr–Nb phase diagram in the vicinity of the α/β transus is a monotectoid with the monotectoid reaction at about 870 K and 20%Nb. The α/β transformation in pure Zr is at about 1135 K, and this is elevated by about

* Corresponding author.
E-mail address: holt@me.queensu.ca (R.A. Holt).

0022-3115/$ - see front matter
doi:10.1016/j.jnucmat.2004.07.043

70 K by commercial levels of oxygen – typically 1000 ppm by wt. In Zr–2.5Nb, the α + β phase field extends from about 870 K to 1200 K [1].

In a previous paper on the role of hot-extrusion on texture development, Holt and Aldridge [9], showed a correlation between the extrusion conditions (extrusion-temperature (923–1123 K), preheat time (0.5–3 h), extrusion ratio/geometry (4:1, 10:1), and billet microstructure (fine, coarse)). The bulk textures of the extrusions, observed by X-ray diffraction (XRD) comprised three components:

1. A predominantly radial [1] component hypothesized to be developed by crystallographic rotation of the α phase due to pyramidal, prism and basal slip. This component is similar to the textures produces by cold working when the wall reduction is significantly greater than the diametral reduction [3,4,10]. This was subsequently shown by Rodríguez [11] to be the texture expected if the predominant deformation mechanism is a combination of prism and pyramidal slip.
2. A predominantly transverse component hypothesized to be associated with the texture developed in the β-phase, the effects of stress on the α/β phase transformation and phase boundary sliding (which results in bodily rotation of the α phase within the β phase). This component is not seen during cold work and cannot be explained by any combination of known slip systems.
3. A predominantly axial component hypothesized to be associated with the texture developed in the β-phase and the α/β phase transformation. This component is associated with a significant volume fraction of β-Zr, present during extrusion, and is also not seen during deformation at any temperature at which the material is predominantly α-Zr.

Standard Zr–2.5Nb pressure tubes are extruded at 1090 K (where the volume fraction of α is something over 50%) with an extrusion ratio of about 10:1. They exhibit mainly the texture Component 2, with the **c**-axes in the radial/transverse plane, predominantly in the transverse direction. This texture is not affected by subsequent 25–30% cold-drawing or stress relief at 670 K for 24 h [9]. The micro-texture (texture which is measured on a crystal to crystal basis) of a standard pressure tube, measured by scanning electron microscopy (SEM) and electron back-scattering diffraction (EBSD) and transmission electron microscopy (TEM) and selected area diffraction (SAD), was reported by Griffiths et al. [12]. It was found that the long axis of the grains as viewed in the radial/transverse plane coincided closely with the **c**-axes (within ±15°), and the distribution of **c**-axes in the radial transverse plane is thus closely related to the orientation of the grain boundaries in this plane. Prior to extrusion these grains are formed from the β-phase on cooling after forging or a β-heat-treatment, they are plate-like [9] and, due to the Burgers relationship [13], the **c**-axis is in the plane of the plate. They remain plate-like as pro-monotectoid α-particles during preheating for extrusion [14], and after extrusion are flattened and folded in the radial/transverse plane, and highly elongated in the axial direction.

The purpose of the current paper is to verify the latter result for a higher temperature of extrusion and to correlate the grain morphology with the three components of texture using SEM EBSD and TEM SAD.

2. Experimental materials and procedures

The materials examined were two extruded tubes, #10 and #20 described in Ref. [9]. These tubes were chosen because they exhibited texture Components 1 and 3. The tubes had an inner diameter of 16 mm and a wall thickness of 4.6 mm and were made with an extrusion ratio of 3.9:1 and a Q ratio (ratio of true strain in the wall thickness direction to that in the circumferential direction) of 2.6, after preheat for 1/2 and 3 h at 1125 and 925 K respectively, for tubes 10 and 20. The billets were machined from 75 mm diameter Zr–2.5Nb rod made from an ingot melted to the specification for Zr–2.5Nb pressure tubes for CANDU reactors, Table 1. Prior to preheating for extrusion, the billet for tube 10 had been β-quenched in oil to give a fine Widmanstätten structure, and that for tube 20 had been slow cooled from the β to give a coarse Widmanstätten structure (see Fig. 2(a) and (b) of Ref. [9]). Tube 20 exhibited a combination of Components 1 and 2, Component 1 being more dominant and tube 10 exhibited mainly Component 2 with a significant amount of Component 3.

Table 1
Chemical specification for Zr–2.5Nb pressure tubes for CANDU reactors (circa 1980)

Niobium	2.4–2.8 wt%
Oxygen	900–1300 ppm by wt.
Hydrogen	<20 ppm by wt.[a]
Iron	<1500 ppm by wt.[b]
Carbon	<270 ppm by wt.
Chromium	<200 ppm by wt.
Tantalum	<200 ppm bt wt.
Zirconium + other permissible impurities	Balance

[a] Changed to <5 ppm by wt. in the mid 1990s.
[b] Changed to <600 ppm by wt in the mid 1980s.

[1] The three principal directions of the tube are defined as radial, transverse and axial in this paper: radial/ transverse and radial/axial are the planes containing the radial and transverse and radial and axial direction respectively.

Table 2
Resolved fraction of basal plane normals in the principal direction for tubes examined in this study

Tube #	F_{radial}	$F_{\text{transverse}}$	F_{axial}
10	0.35	0.44	0.21
20	0.55	0.38	0.07

Table 2 gives the previously reported resolved fractions of basal plane normals in the three principal directions of the tubes, F_d, defined by:

$$F_d = \sum_{\theta} V(\theta)\cos^2\theta,$$

where d is the direction (radial, transverse, axial) and $V(\theta)$ is the volume fraction of material with its **c**-axis at an angle θ from the d direction.

The samples for SEM and EBSD (electron backscattered diffraction) were prepared by cutting the tubes normal to axial direction (i.e. the face examined is transverse cross section), mechanical polishing and electropolishing in 5% perchloric acid + 60% methanol + 35% butycellosolve at −45 °C and 20 V. They were examined on a JEOL 840 SEM equipped with an HKL backscattered electron camera and an automated data acquisition and analysis software (Channel 5). The resolution of the JEOL 840 is about 1 μm, so that the finest grains are not sampled. In EBSD experiments, the samples were positioned in the chamber such that the three directions of the tubes (radial, transverse and axial) corresponded to the coordinates in the pole figures, X_0, Y_0 and Z_0, respectively. The scanning step size and the time per cycle in EBSD acquisition were set to be 0.2 μm and 0.160 s, respectively. An SEM image, the corresponding crystallographic mapping and pole figures were produced for each examined area. The angles between the **c**-axes and the grain boundaries of elongated pro-monotectoid α grains in the radial/transverse plane were determined by measuring the angle between the α-grain boundaries and radial direction on SEM micrographs, and the Euler angles of the same α grain. The distributions of the angles between the long axes of the grains and the radial directions of the tubes were also measured on SEM micrographs.

The TEM thin foils having normals parallel to the axial and transverse directions of the tube were prepared to study the microstructural details and crystallographic orientation of both pro-monotectoid α grains and transformed β (α bundles in Tube #10). Slices of 150–250 μm thick were cut normal to either axial or transverse direction and the discs of 3 mm in diameter were punched, followed by twin-jet electro-polishing in 5% perchloric acid + 95% methanol at −50 °C and 20 V. The thin foils were observed using a Philips CM 20 at 200 kV. Double tilt sample holder (α tilt: ±50° and β tilt: ±30°) was used to determine the crystallographic orientation of different α grains by matching the image and diffraction patterns taken when the two tilt angles were recorded. The distribution of the angle between **c**-axis and pro-monotectoid α-grain boundaries in radial/transverse plane of Tube #20 was obtained by examining a large number of α-grains in different areas of different thin foils. For thin foils of Tube # 10, the orientation of **c**-axis of the transformed α-bundles with respect to the axial direction was recorded, and the angle between **c**-axis and the pro-monotectoid α-grain boundaries was measured also. The thin foils normal to the transverse directions of the two tubes were also examined to reveal the microstructures in the radial/axial plane.

3. Results

3.1. Microstructures

In the radial/axial plane, Tube 20 comprised mainly elongated grains containing a relatively high density of **c**-component and **a**-type dislocations (Fig. 1(a)). When viewed in the radial/transverse plane of the tube, the grains were flattened and often folded, the long axes making a range of orientations relative to the transverse and radial directions of the tubes (Fig. 1(b)).

In the radial/axial plane Tube 10 exhibited a large proportion of elongated grains which clearly arise from deformation of the pro-monotectoid grains present at the extrusion temperature, prior to extrusion, but also a significant proportion (~50%) of grains not aligned with the axial direction of the tube, Fig. 2(a). These latter grains often occurred in 'colonies' or parallel groupings. In the radial-transverse plane the microstructure comprised many flattened, folded grains, similar to those in Tube 20, but with lower dislocation densities (Fig. 2(b)). It also showed misaligned colonies similar to those observed in the radial axial plane. For the most part, the colonies of grains in Tube 10 exhibited very low dislocation densities when imaged using $\mathbf{g} = (0002)$, as in Fig. 2(b), and when imaged using $\mathbf{g} = \{10\bar{1}1\}$. This indicates that the densities of both **c**-component and **a**-type dislocations are low and, therefore, that the α colonies were formed by transformation from β to α after extrusion.

3.2. Bulk textures

The (0002) pole figures determined by EBSD are shown in Figs. 3 and 4 and the F_d's are shown in the upper right corner of the figures, where x = radial, y = transverse and z = axial. Tube 20 (Fig. 3) showed a predominance of Component 1 for the section examined, greater than had been observed over a much larger sample using X-ray diffraction. Tube 10 (Fig. 4) showed a predominance of Component 2, with a substantial proportion of Component 1 and a significant proportion of

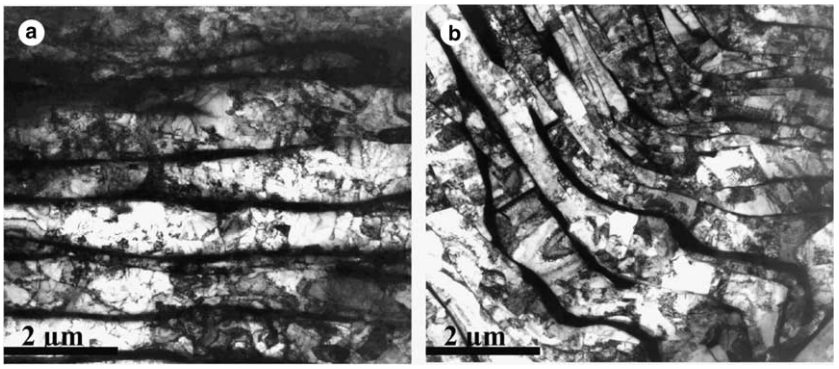

Fig. 1. Microstructure of Tube 20 observed by TEM in radial-axial section (a) and in radial-transverse section (b). The axial and transverse directions of the tube are close to horizontal respectively in (a) and (b).

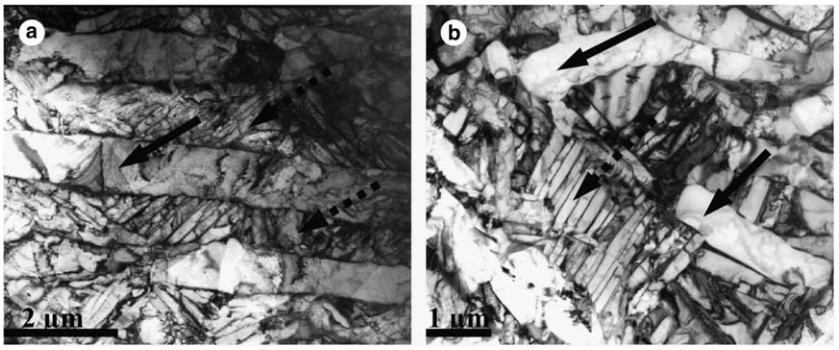

Fig. 2. Microstructure of Tube 10 observed by TEM in radial–axial section (a) and in transverse cross-section (b) and showing promonotectoid α (arrows) and transformed β (broken arrows).). The axial and transverse directions of the tube are close to horizontal respectively in (a) and (b).

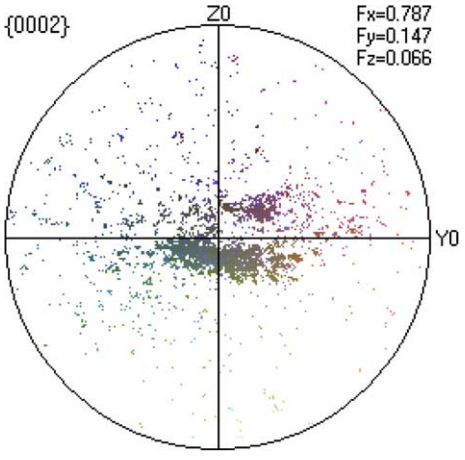

Fig. 3. (0002) pole figure determined by EBSD for Tube 20 (x = radial, y = transverse, z = axial).

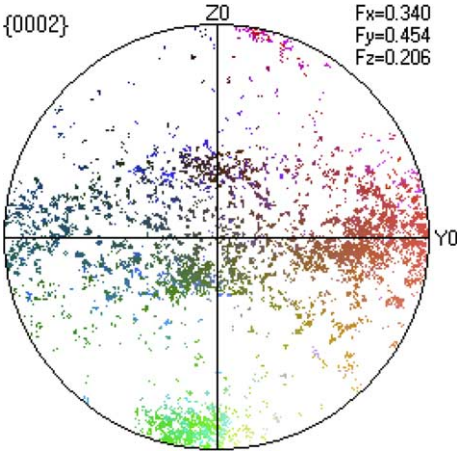

Fig. 4. (0002) pole figure determined by EBSD for Tube 10 (x = radial, y = transverse, z = axial).

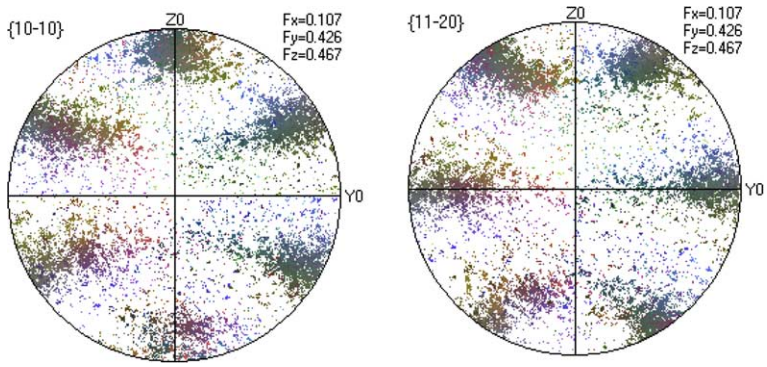

Fig. 5. Prism pole figures determined by EBSD for Tube 20 (x = radial, y = transverse, z = axial).

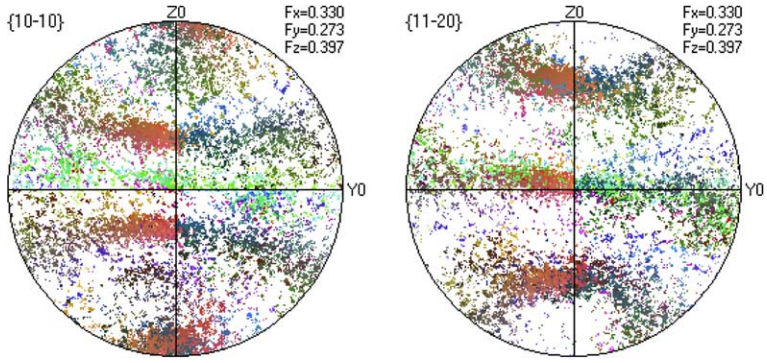

Fig. 6. Prism pole figures determined by EBSD for Tube 10 (x = radial, y = transverse, z = axial).

Component 3. In this case the F_d's agreed fairly well with the earlier X-ray data.

The prism pole figures determined by EBSD are shown in Figs. 5 and 6. In both cases $\{10\bar{1}0\}$ is aligned with the tube axis. In Tube 20 $\{10\bar{1}0\}$ and $\{11\bar{2}0\}$ are distributed at 60° intervals in the axial/transverse plane with a 30° offset, corresponding to Component 1 of the (0002) texture. Tube 10 shows bands of $\{10\bar{1}0\}$ at 30° from the radial/transverse plane and bands of $\{11\bar{2}0\}$ 30° away from $\{10\bar{1}0\}$ corresponding to radial/transverse spread of (0002). There are also weaker bands of $\{10\bar{1}0\}$ and $\{11\bar{2}0\}$ in the radial/tranverse plane corresponding to Component 3 (crystals with (0002) in the axial direction, Fig. 7).

3.3. Micro-textures

Figs. 8 and 9 show the distribution of the angle between the **c**-axis and the long dimension of each grain examined as viewed in the radial/transverse plane. The data in Fig. 8 were obtained by TEM/SAD and those in Fig. 9 by SEM/EBSD. The data obtained by both techniques are similar, exhibiting broad maxima 20–40° on each side of the origin. Figs. 10 and 11 show the equivalent data for Tube 10, for the elongated (pro-monotectoid) α-grains. In contrast to the case of Tube 20, the data for Tube 10 are clustered within 10–20° of the origin.

Of 87 colonies of misaligned grains examined by TEM/SAD in Tube 10, 76 had a [0001] zone axis within about 15° of the axis of the tube, corresponding to Component 3 of the texture (Fig. 12). The remaining 11 had a range of pyramidal and prism zone axes (Table 3).

3.4. Grain-axis orientations

Figs. 13 and 14 show the distribution of angles between the long axis of the pro-monotectoid α-grains and the radial direction as observed in radial/transverse section (Figs. 1(b) and 2(b)). In Tube 20 there is a very pronounced maximum in the transverse direction similar to that observed in pressure tubes [12]. Tube 10 has a less pronounced maximum in the transverse direction.

4. Discussion

The pole figures derived from the SEM/EBSD examination of tube are consistent with the previous observations using XRD [9], and clearly show the existence of

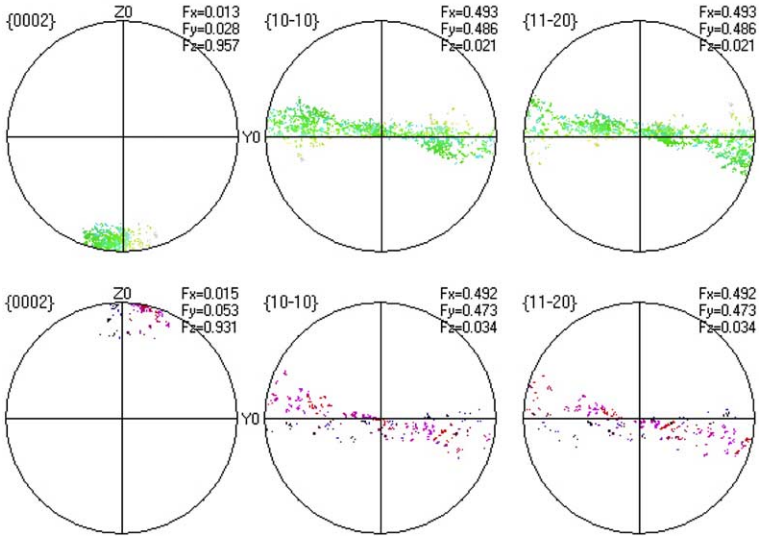

Fig. 7. $\{10\bar{1}0\}$ (middle) and $\{11\bar{2}0\}$ (right) pole figures for Tube 20 corresponding to Component 3 (grains with their **c**-axis aligned with the tube axis as shown on the left – here, x = radial, y = transverse, z = axial).

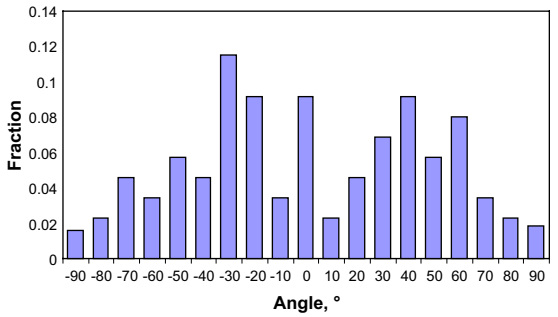

Fig. 8. Distribution of the angle between **c**-axes and long axes of α-grains in the radial/transverse plane of Tube 20 determined by TEM SAD.

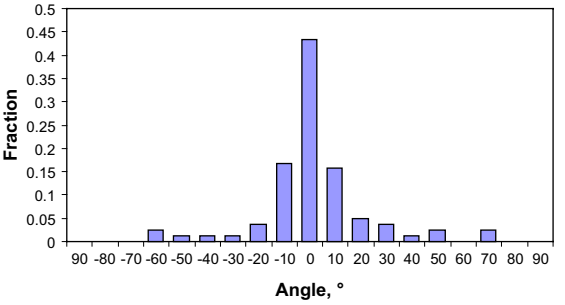

Fig. 10. Distribution of the angle between **c**-axes and long axes of promontectoid α-grains in the radial/transverse plane of Tube 10 determined by TEM SAD.

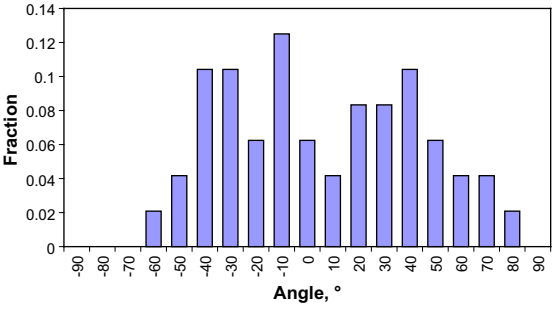

Fig. 9. Distribution of the angle between **c**-axes and long axes of α-grains in the radial/transverse plane of Tube 20 determined by SEM EBSD.

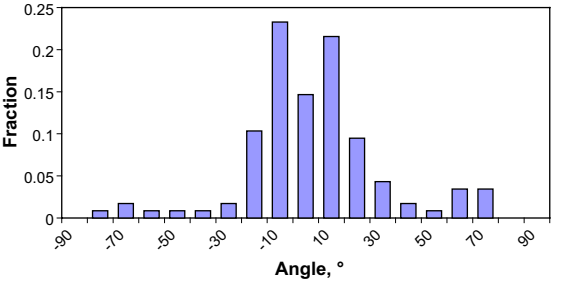

Fig. 11. Distribution of the angle between **c**-axes and long axes of pro-monotectoid α-grains in the radial/transverse plane of Tube 10 determined by SEM EBSD.

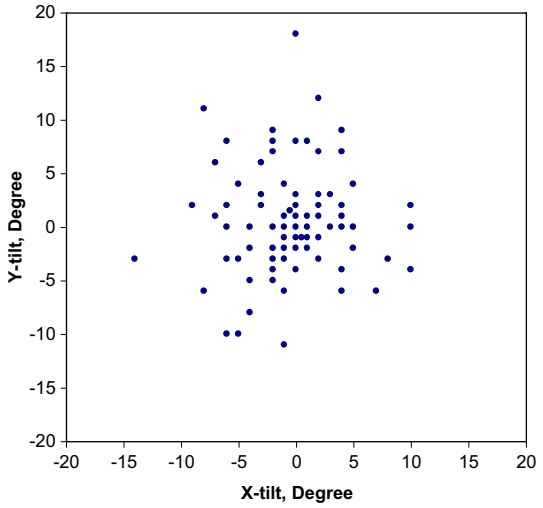

Fig. 12. Distribution of [0001] zone axis with respect to the electron beam direction (axial direction of Tube 10) in TEM for 76 of 87 measurements of α-bundles.

Table 3
Zone axes and deviation from axial direction of Tube 10 for 11 α-bundles with zone axes other than [0001]

Zone axis	*X*-tilt (°)	Y-tilt (°)
[2201]	−8	−5
[2201]	13	2
[0110]	−1	−6
[0110]	2	6
[0110]	−8	2
[0110]	−12	−4
[4401]	4	0
[3301]	3	4
[1211]	6	−3
[1213]	2	−6
[1213]	4	−2

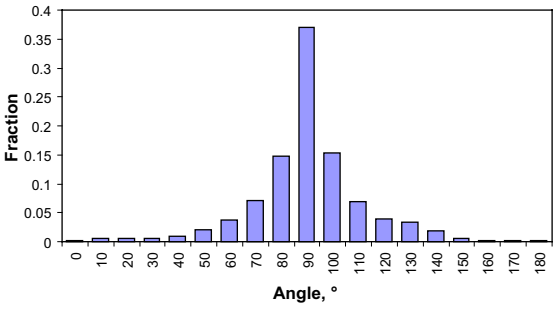

Fig. 13. Distribution of the angle between the long axis of the promonotectoid α-grains and the radial direction in the radial/transverse plane of Tube 10.

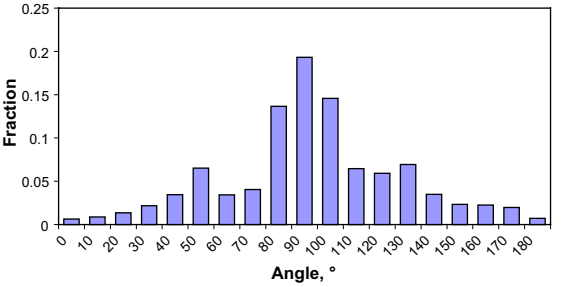

Fig. 14. Distribution of the angle between the long axis of the promonotectoid α-grains and the radial direction in the radial/transverse plane of Tube 20.

three dominant components of texture. Combining this with the TEM/SAD data we see that Components 1 and 2 occur in the elongated α grains, with component 1 dominant at lower extrusion temperature and component 2 dominant at higher extrusion temperature. Component 3 occurs only in the misaligned colonies of grains and is dominant in these grains. The difference between the pole figure for Tube 20 derived from SEM/EBSD, and that previously reported from XRD (the former contains a higher proportion of basal plane normals in the radial direction) may relate to sampling errors because the finest grains are not sampled by EBSD. Also, although many points were sampled by EBSD (>20000), only of the order of 100 distinct grains were sampled, so that there may also be a statistical error.

The elongated grains in both tubes are clearly those present as pro-monotectoid α before extrusion. They originate from the β heat treatment prior to extrusion and represent the majority of the structure on preheating for extrusion at 925 K, and perhaps 20–40% of the structure on heating at 1125 K prior to extrusion. Because these grains are formed during the α/β phase transformation, they are expected to exhibit the Burgers relationship to the prior $\beta\{11\bar{2}0\}_\alpha \| \{111\}_\beta, \langle 0001\rangle_\alpha \| \langle 011\rangle_\beta$, with a habit plane of $\{11\bar{2}0\}_\alpha \| \{112\}_\beta$ [15]. The **c**-axis, and $\{10\bar{1}0\}_\alpha$ are thus in the plane of the plate. That the Burgers relationship holds in these circumstances was clearly seen in the development of texture in heat-treated Zr–2.5Nb pressure tubes [16]. Prior to extrusion, the texture is approximately random [9].

After extrusion the **c**-axis of these grains is rotated into the radial/transverse plane in both tubes, however the alignment associated with Component 2 (Tube 10) is more pronounced, and there is clearly a transition in the mechanism with extrusion temperature, the **c**-axis no longer being in the plane of the plate in Tube 20, but remaining in the plane of the plate in Tube 10. The former has the texture expected for material that has deformed by prismatic, basal and pyramidal slip. This has been clearly demonstrated by modeling texture

development during rolling of Zr by Rodríguez [11], the rotation occurring relative to the orientation of the boundaries, in the conventional manner, by slip, within the individual grains.

The texture of the elongated α grains in Tube 10, is the predominant component in CANDU pressure tubes. The fact that the **c**-axis remains within the plane of the plate suggests that little pyramidal slip is occurring. Previously, it was hypothesized that this component could develop, at least partially by the bodily rotation of the α plates within the β matrix, it being well established that in Zr alloys, β-Zr is much softer than α-Zr in the temperature range of interest, e.g., Ref. [17]. This mechanism would tend to align the **c**-axis in the wall of the tube, but not specifically into the transverse direction – which would require simultaneously, a rotation of the plate about its own normal. The answer may lie in the mechanism of rotation, which would require not only a much higher strain rate in the β- than in the α-phase, but also shear (sliding) along the α/β phase boundaries. A study of the boundary dislocation structure might reveal more about possible mechanisms of this rotation. An alternative explanation is preferred growth and shrinkage of variants of the α orientation, in response to the strains imposed during extrusion (radial strain = −0.98, transverse strain = −0.38). Note that Rodríguez [18] concluded that the phase transformation was *not* involved in texture development in Zr–2.5Nb at 1125 K in uniaxial tests on cylinders, based on the texture of a specimen of β_{Zr} (Zr–20Nb) deformed under the same conditions as the Zr–2.5Nb, which showed no correlation of $\{1\,1\,0\}_\beta$ with $(0\,0\,0\,2)_\alpha$. This may be misleading since the slip mechanisms may be affected by the Nb content (that of the β-phase in Zr–2.5Nb at 1125 K is <10%) and the strain path of the β-phase in the duplex alloy may be different from that in the single phase alloy. In pressure tubes, the texture of the β-phase measured in situ is a $\{0\,0\,1\}_\beta$, $\langle 1\,1\,0\rangle_\beta$ 'rolling texture' [19]. This contains variants of $\{1\,1\,0\}_\beta$ that coincide with α-texture Components 2 and 3. The strains derived for the Burgers relationship during transformation from β to α [13] are:

- contraction of about 13% along $\langle 1\,1\,\bar{2}\,0\rangle_\alpha$, corresponding to $\langle 0\,0\,1\rangle_\beta$ or the radial direction;
- expansion of about 6% along $\langle 1\,\bar{1}\,0\,0\rangle_\alpha$, corresponding to $\langle 1\,1\,0\rangle_\beta$ or the axial direction;
- contraction of 2% along $[0\,0\,0\,2]_\alpha$, corresponding to $\langle 1\,\bar{1}\,0\rangle_\beta$ or the transverse direction.

The strain would favor the development of an α-variant corresponding to Component 3 at the expense of other variants.

It is now clear, from the very low dislocation density observed in the Widmanstätten colonies, that Component 3 of texture (**c**-axis in the axial direction of the tube) is formed after extrusion, during the β to α transformation upon cooling. Again, there appears to be a preferred variant of the transformation, but the stresses imposed by the extrusion tooling are now relaxed. The factors that could potentially influence the transformation are the differences in thermal expansion between the two phases, and the constraints imposed by the much stronger, highly elongated, α-grains. The large thermal expansion coefficient along the **c**-axis would induce compression along the transverse direction in the β-phase, $\langle 1\,\bar{1}\,0\rangle$, but this direction does not experience a large contraction during transformation, and also any differential expansion would be very small ($\ll$1%) compared with the transformation strains. Alternatively, the potential expansion along $\langle 1\,\bar{1}\,0\,0\rangle_\alpha$, or contraction along $\langle 1\,1\,\bar{2}\,0\rangle_\alpha$ would be severely constrained in the axial direction because of the fiber reinforcing effect of the aligned α-grains. Corresponding with the prism pole figures for Component 3, Fig. 7, the weaker alignment of the α-grains in the transverse direction would offer less constraint corresponding to the intermediate strain along $\langle 1\,1\,\bar{2}\,0\rangle_\alpha$. The least constraint would be in the radial direction corresponding to the large expansion along $\langle 1\,\bar{1}\,0\,0\rangle_\alpha$.

5. Conclusions

Pole figures determined by SEM/EBSD for extruded Zr–2.5Nb tubes correspond reasonably well with bulk pole figures previously determined by X-ray diffraction (XRD).

Three components of texture are seen to correlate with the shape and morphology of the α-grains and their contained dislocation substructures. The first component corresponds to elongated alpha grains containing a high density of **a** and **c** + **a** dislocations in which the **c** axis is oriented at a relatively high angle to the long dimension of the α-grains as viewed in transverse section; these grains comprise a texture component with the **c**-axis in the radial transverse plane, tilted towards the radial direction. The second component corresponds to elongated α-grains containing a low dislocation density in which the **c**-axis is oriented parallel to the long dimension of the alpha grains in radial transverse section: these grains also comprise a texture component with the **c**-axis in the radial/transverse plane, but predominantly in the transverse direction. The final component corresponds to colonies of Widmanstätten-like α-grains that are transformed from the β-phase: the majority of these grains have their **c**-axes in the axial direction. These grain have very low dislocation densities and are probably developed upon cooling after, extrusion.

The appearance of these components is attributed to combinations of **a** and **c** + **a** slip within the α-phase (Component 1) and the effects of stress (Component 2)

and constraint (Component 3) on the β to α phase transformation during and after extrusion respectively.

Acknowledgment

Funding for this work was provided by the Natural Sciences and Engineering Research Council of Canada, Ontario Power Generation Inc. and the CANDU Owners Group Inc. under an Industrial Research Chair in Nuclear Materials at Queen's University. The authors thank M. Griffiths and R.D. Sage of AECL, Chalk River Laboratories for providing archive specimens from the earlier studies [9].

References

[1] B.A. Cheadle, in: Proceedings of 3rd International Symposium on Zirconium in the Nuclear Industry, ASTM STP 633, 1977, p. 457.
[2] B.A. Cheadle, S.A. Aldridge, C.E. Ells, Can. Metall. Quart. 11 (1972) 121.
[3] D.O. Hobson, ASTM STP 458, 1969, p. 37.
[4] E. Tenckhoff, P.L. Rittenhouse, ASTM STP 458, 1969, p. 50.
[5] B.A. Cheadle, ASTM STP 458, 1969, p. 68.
[6] W.K. Alexander, V. Fidleris, R.A. Holt, in: Proceedings of 3rd International Symposium on Zirconium in the Nuclear Industry, ASTM STP 633, 1977, p. 344.
[7] C.E. Coleman, in: Proceedings of 5th International Symposium on Zirconium in the Nuclear Industry, ASTM STP 754, 1982, p. 393.
[8] M.L. Picklesimer, J. Electrochem. Technol. 4 (1966) 289.
[9] R.A. Holt, S.A. Aldridge, J. Nucl. Mater. 135 (1985) 246.
[10] K. Kalström, Can. Metall. Quart. 11 (1972) 185.
[11] A. Salinas Rodríguez, PhD thesis, McGill University, Montreal, PQ, Canada, 1988.
[12] M. Griffiths, R.A. Holt, J. Li, S. Saimoto, Microstruct. Sci., ASM Int. 26 (1999) 293.
[13] W.G. Burgers, Physica 1 (1934) 561.
[14] R. Choubey, S.A. Aldridge, J.R. Theaker, C.D. Cann, C.E. Coleman, in: Proceedings of 11th International Symposium on Zirconium in the Nuclear Industry, ASTM STP 1295, 1996, p. 657.
[15] G.T. Higgins, E.E. Banks, J. Electrochem. Technol. 4 (1966) 341.
[16] B.A. Cheadle, C.E. Ells, J. Electrochem. Technol. 4 (1966) 329.
[17] H.E. Sills, R.A. Holt, in: Proceedings of 4th International Symposium on Zirconium in the Nuclear Industry, ASTM STP 681, 1979, p. 325.
[18] A. Salinas Rodríguez, Acta Metall. Mater. 43 (1995) 485.
[19] M. Griffiths, C.K. Chow, C.E. Coleman, R.A. Holt, S. Sagat, V.F. Urbanic, in: Proceedings of 16th International Symposium on Effects of Radiation on Materials, ASTM STP 1175, 1993, p. 1077.